Optimization of the xNTD configuration

T.J. Cornwell, ATNF

Tim.Cornwell@csiro.au

4/9/06

Abstract: *I consider the design of the xNTD configuration for site B at Mileura. I advocate that the naturally weighted PSF, tapered by the primary beam, should be close to a Gaussian. I describe an algorithm for optimizing the configuration with this goal. I propose a configuration capable of excellent imaging at about 30 arcsecond resolution at 1.4GHz. I also discuss the options for later expansion.*

1. xNTD Goals and challenges

The xNTD has two main purposes – to act as a demonstrator for the Square Kilometer Array and to do great science. The xNTD will be a novel type of radio telescope – consisting of about 30 – 50 conventional synthesis arrays operating in parallel.

Johnston (2005) has summarized the xNTD science requirements, drawing on a workshop held at the ATNF in April 2005. In a recent note, Johnson (2006) summarizes the various resolution drivers, and selects resolution of about 30 arcsec. Staveley-smith (2006) presents a detailed analysis of the needs for HI surveys for which 30 arcsec is optimum. Here I distill only the core performance requirements.

Table 1 Summary of possible xNTD science

Topic	***Requirements***
Extragalactic HI emission surveys	300 day all sky survey. Ultra deep, 100 day integration in one direction.
Extragalactic HI absorption surveys	Large scale survey, tens of days, to 0.01 optical depth
Survey for OH masers and mega masers	100 day survey over 1000 square degrees
Continuum surveys	NVSS equivalent every day. 1 day gives 400uJy noise (confusion limit), can see polarization variability deeper. Variability at 2% for 100mJy sources, 20% for 10mJy, daily.
Galactic HI surveys	100 day survey, 600 square degrees at 1K, 40 arcsec. Deep imaging of mid-latitudes for HVCs: 100mK at 3 arcmin
Pulsar surveys	120 day all sky survey, adding all collecting area, pixelizing the primary beam
Polarization and Cosmic Magnetism	All sky survey to 1% across the field. Faraday tomography: slices of 100MHz across entire band
VLBI	Wide field of view, ionospheric calibration

Table 2 xNTD telescope parameters

	xNTD
Antennas	30 of 12m 20 of 15m
Frequency Range	0.8 – 1.7 GHz
Polarizations	2
Bandwidth	300MHz
Frequency resolution	20kHz
Spectral Channels per beam	16384
A_{eff}/T_{sys}	3584/50 = 76
Field of view	40 deg^2

This argument establishes the typical baseline length – about 1-2km. I will also consider a possible upgrade to the array to double the baseline length and collecting area.

Next I consider the question of the best layout of antennas.

2. Linear mosaic imaging model

To determine the antenna layout, I have to understand how the telescope will image with

those antennas. The xNTD is primarily a parallel mosaicing machine. That it is parallel rather than sequential aids calibration and improves survey speed but it does not change the basics of how the telescope measures the sky brightness. Hence we can use conventional mosaicing theory (Cornwell, 1988; Cornwell, Holdaway, and Uson, 1993). The visibility measured between two antennas *i* and *j* pointing at location *p* is:

$$V_{ij,p} = \int E_{i,p} E^*_{j,p} I(l,m) e^{2\pi j\left(u_{i,j}l + v_{i,j}m\right)} dldm$$

The voltage pattern *E* of a beam is given by the sum of the voltage patterns of a set of element voltage patterns.

$$E_{i,p} = \sum_k w_{p,k} E^{el}{}_{i,k}$$

$$V_{ij,p} = \int \sum_{k,l} w_{p,k} w_{p,l}{}^* E_{i,k}{}^{el} E_{j,l}{}^{el^*} I(l,m) e^{2\pi j\left(u_{i,j}l + v_{i,j}m\right)} dldm$$

$$A_{ij,p}(l,m) = \sum_{k,l} w_{p,k} w_{p,l}{}^* E_{i,k}{}^{el} E_{j,l}{}^{el^*}$$

Suppose that we form dirty image and dirty PSF from the measured visibilities by the standard process.

$$I^D(l,m) = \mathrm{Re}\left[\sum w_{ij} V_{ij,p} e^{2\pi j\left(u_{i,j}l + v_{i,j}m\right)}\right]$$

$$B(l,m) = \mathrm{Re}\left[\sum w_{ij} e^{2\pi j\left(u_{i,j}l + v_{i,j}m\right)}\right]$$

We can then calculate an optimum estimate of the sky from by a "linear mosaic" of the dirty images:

$$I^{LM}(l,m) = \frac{\sum_p A_p(l,m) I^D_p(l,m)}{\sum_p A_p{}^2(l,m)}$$

If the point spread functions *B(l,m)* are identical (a good approximation for a focal plane array enabled telescope), then an approximate convolution equation holds:

$$I^{LM}(l,m) \approx B^{LM}(l,m) * I(l,m)$$

The effective (linear mosaic) point spread function is given by:

$$B^{LM}(l,m) = B(l,m)\frac{\sum_p A_p(l,m)A_p(l=0,m=0)}{\sum_p A_p{}^2(l,m)}$$

For many purposes, the linear mosaic of the dirty images will suffice. We expect, for example, that for HI emission searches, spectral line images will be formed by calculating the linear mosaic from continuum subtracted visibility data. If deconvolution is needed, as will be the case for continuum imaging, the linear mosaic of the residual visibility data can drive the iteration. In either case, the linear mosaic PSF describes the imaging performance of the array.

3. Array configuration design

Since xNTD is primarily a survey telescope, we should optimize the coverage correspondingly. To optimize sensitivity, we require Fourier plane coverage that when naturally weighted leads to an acceptable point spread function needing little deconvolution. Since the clean PSF is usually a Gaussian, this means that the naturally weighted PSF should be matched to a Gaussian. Equivalently, the sensitivity function in the Fourier plane should be a Gaussian giving the required resolution. For images needing little or no deconvolution, such as spectral cubes, it still pays to have a well-defined point spread function so that flux estimates are reliable. In addition, source-finding algorithms such as Sextractor (continuum) and Duchamp (spectral line) will almost certainly benefit from a well-behaved noise correlation matrix.

Furthermore, xNTD is a wide-field mosaicing telescope, using either a FPA or perhaps a cluster of horns. Hence the relevant PSF is that for linear mosaicing $B^{LM}(l,m)$.

Finally, there is the question of whether to optimize the monochromatic or broadband coverage. Since the most demanding imaging is that of the continuum, we choose to optimize the coverage over the full bandwidth. The effect of this choice is to cluster the inner antennas somewhat closer since the longer spacings are well sampled over the bandwidth.

This then completes the optimization criterion – we will match the broad band, naturally weighted PSF, multiplied by the primary beam, to a Gaussian of a given resolution. This already yields an interesting constraint – if the synthesized beam is to be roughly a Gaussian then the maximum baseline must about 2 times the typical scale size. So for a scale size of about 1km, we may need baselines up to 2km. This necessity has been ignored so far and either leads to less resolution for a given maximum baseline or to a longer maximum baseline for a given resolution. This argument shows that the computing will be substantially more demanding than calculated on the basis of the scale size and maximum baseline both being 1km (Cornwell, 2005). The computing scales roughly as the square of the baseline, so the cost would increase by about a factor of four.

The Gaussianicity requirement rules out approximately scale free configurations such as logarithmic spirals. Scale-free configurations give an excess of short spacings and

therefore lead to point spread functions with broad wings. The VLA configuration has a similar nature, leading to problems when imaging large structures.

Another fairly obvious conclusion is that multi-frequency synthesis and more antennas may be needed to provide adequate Fourier plane coverage. Thus 30 antennas of 12m diameter would be better than 20 antennas of 15m diameter (assuming that the overall field of view is fixed).

In summary, the optimization must find the set of antenna locations *(x,y)* that minimizes the sum squared error between the naturally weighted beam and desired beam.

$$S = \int A(l,m)\left(B^G(l,m) - \mathrm{Re}\left[\sum w_{ij} e^{2\pi j\left((x_i - x_j)l + (y_i - y_j)m\right)}\right]\right)^2 dldm$$

I have chosen to use the square so that a gradient search is easily performed. Other norms could be used at the cost of more complicated search algorithms. This approach is similar to that developed by Boone (2001).

To perform the detailed optimization of the array layout, we have two routes – first, I have written a python program, *harry*, to perform a gradient search in *S*, and second, Mattieu de Villiers of the Karoo Array Telescope has kindly provided us with a copy of his optimization program, AntConfig. The python program is simple and single-minded, and allows quick experimentation with different approaches. de Villier's program, AntConfig, is (much) faster, interactive, and generally easier to use, so I have tended to use it for the production work but I do cross check general conclusions with *harry*. More details on *harry* are given in an appendix. A paper on AntConfig is in preparation by de Villiers.

The characteristic details of layouts found using this approach are that most antennas are located around an envelope, with a few locations interior to the envelope, and there are no obvious symmetries.

4. Geographical constraints

The xNTD could potentially be located anywhere on Mileura station. Oberoi (2006) has examined the various constraints on location of the LFD and xNTD at Mileura in some detail. Using a model whereby LFD and xNTD are located adjacently and share infrastructure, he proposes two sites, A and B, on somewhat elevated terrain. The location of the sites is shown in the next two figures. Oberoi's model works for a small configuration xNTD but not for the longer baselines considered here. In addition, neither of the two sites seems able to support the LFD requirement of a site that is coplanar to within 1 meter. Hence I have considered only models where xNTD and LFD are separately located. Such a model also has advantages for limiting the RFI from one telescope to the other.

Site B is closest to the center of the Radio Astronomy Park and I consider that as the

prime site for xNTD. The road access is somewhat better than for Site A – which may be more important for xNTD because of the larger physical size and mass of the antennas.

Site B, as all of Mileura Station, is quite flat. The gradients are about 3-4 m per kilometer on average.

The environmental constraints are those found in a study by Holm and Associates (2005). This study identified regions where vegetation risk precludes antenna location. A map from this study was scanned and converted to a mask for use in the AntConfig program.

In addition, we also made a trip to the sites listed below and made a visual investigation of all suggested antenna locations.

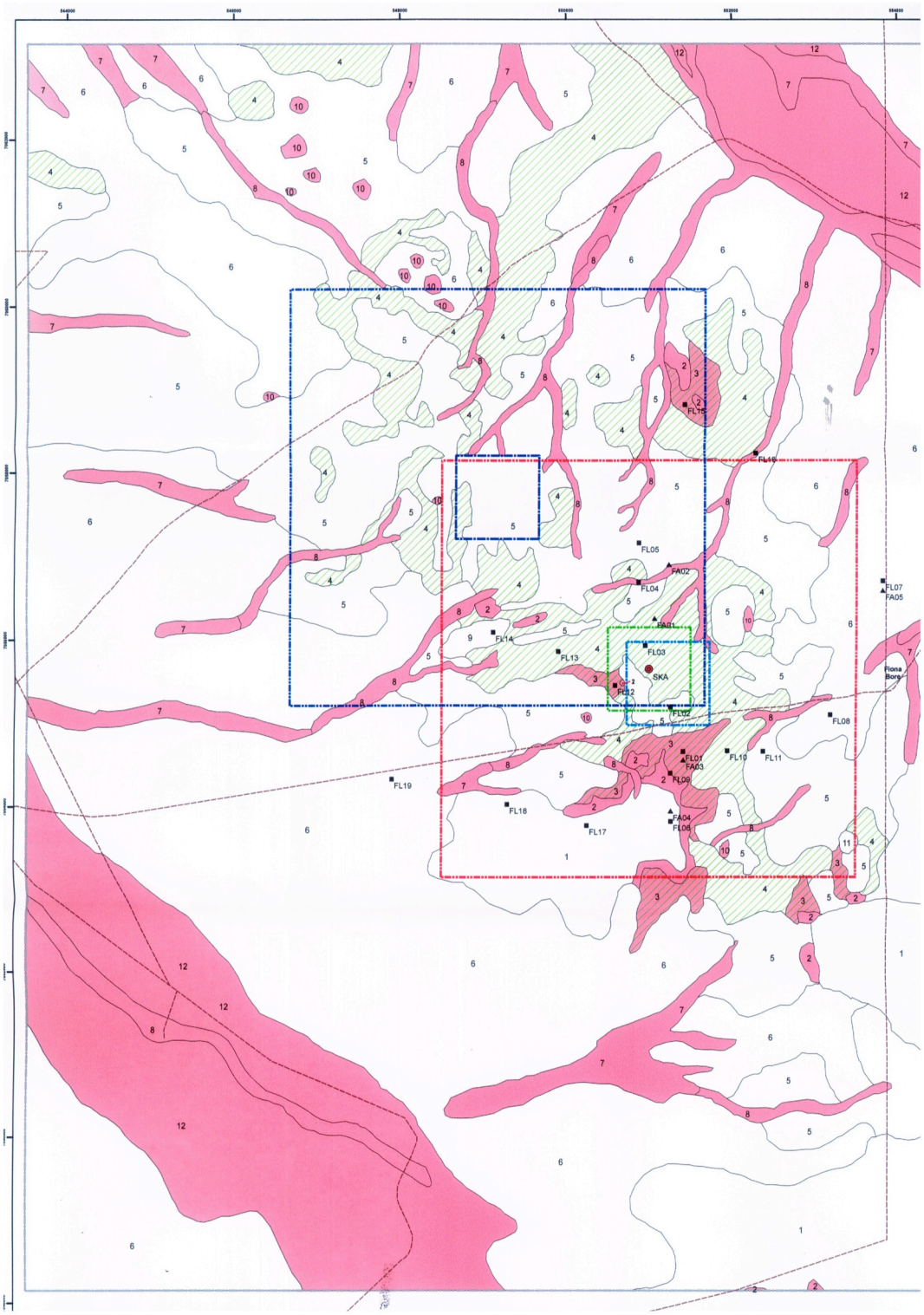

Figure 1 Holm and Associates study map.

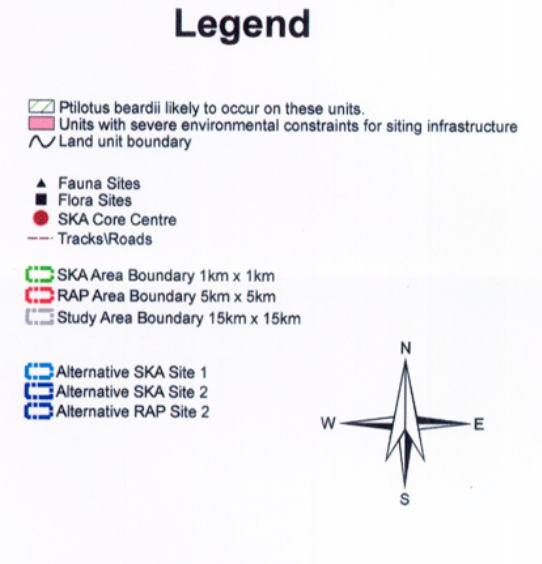

Figure 2 Caption for Holm and Associates map

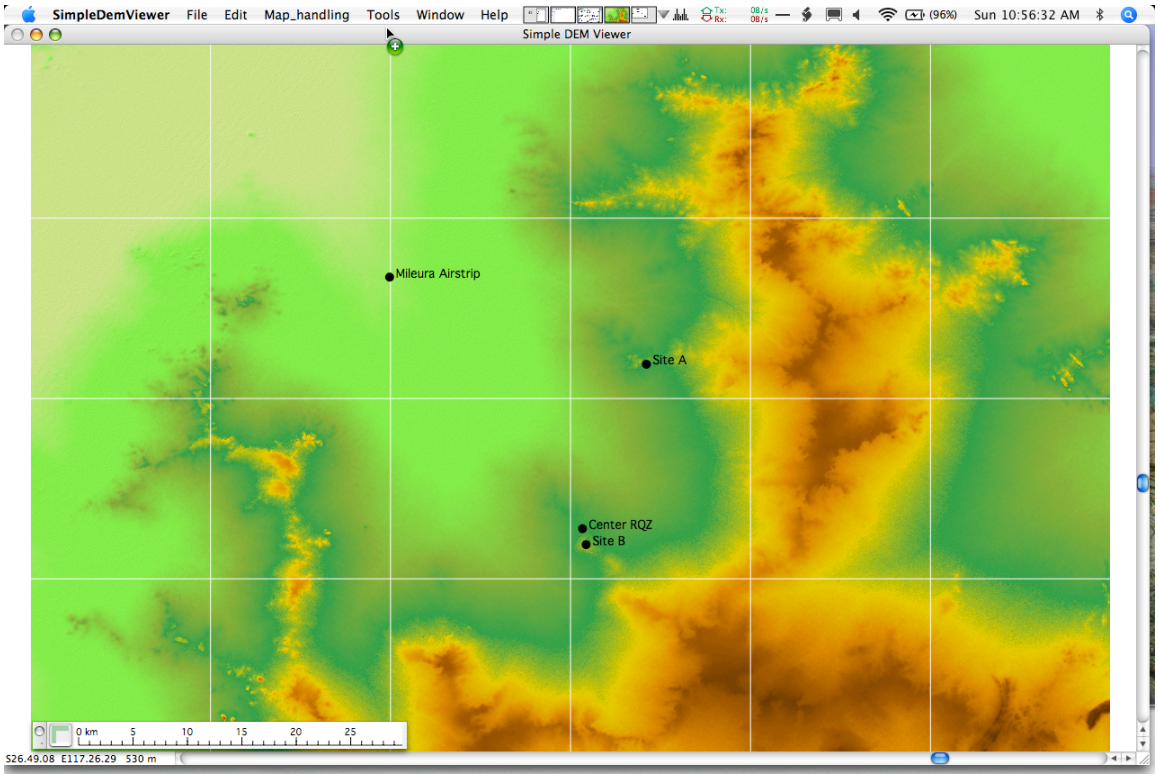

Figure 3 Digital elevation model of Mileura site. Colors range to 400m to 540m elevation above sea level. The data file is in the NTD subversion repository
http://sourcecode.atnf.csiro.au/repos/NTD/configurations/resources/S27E117.hgt

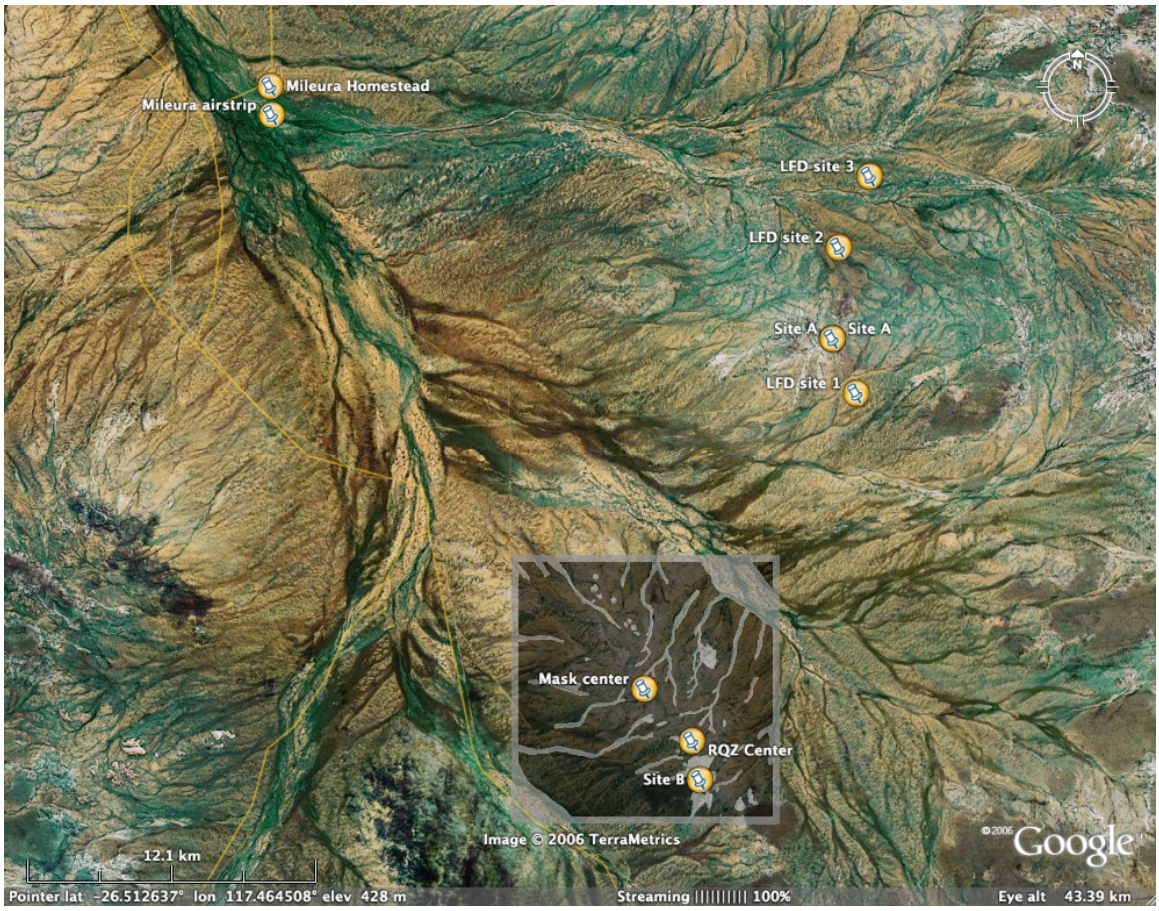

Figure 4 Google Earth map of Mileura station, showing Oberoi's Sites A and B, LFD sites 1, 2, and 3, and the environmental survey area around the Radio Astronomy Park.
http://sourcecode.atnf.csiro.au/repos/NTD/configurations/resources/Mileura.kmz

Figure 5 Environment constraints (from Holm and Associates, 2005) superimposed on Google map. Light areas are not to be used for antenna sites. The enclosing green box is 10,800m across (inside edges), and spans 500 pixels in the mask image.

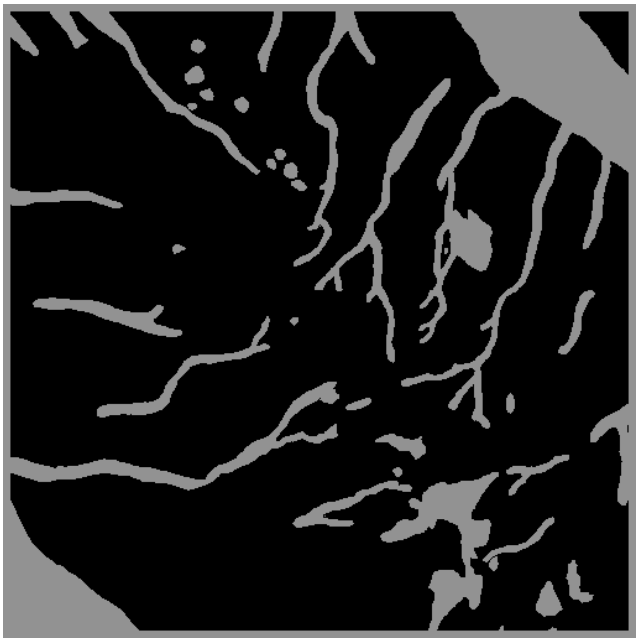

Figure 6 Mask for AntConfig. Antennas are allowed only in the black regions

Table 3 Selected reference positions

Location	***Longitude***	***Latitude***
Mileura homestead	117°19'57.69"E	26°22'20.79"S
Center RQZ	117°34'13.00"E	26°28'6.00"S

Oberoi Site A	117°34'13.00"E	26°28'6.00"S
Oberoi Site B	117°30'52.00"E	26°38'6.00"S
Mask center	117°29'27.64"E	26°36'2.86"S
Correlator site	117°30'45.00"E	26°37'1.00"S

5. Results

There is no single solution to the optimization problem – by starting from different points, one finds quite different solutions. The overall properties are the same – the envelope and the quasi-random distribution of points internally – but the details differ. This indeterminacy allows adaptation to the local geography – a satisfactory array should be possible provided most of the telescope location is available. However, the envelope is close to a Releaux triangle (as found by Keto, 1997). It would be convenient for cable routing if this triangle did not traverse forbidden regions too often. Regions at Site B fitting this extra criterion are centered at the mask center and a few kilometers to the northwest.

The next figure shows a configuration optimized for 8 hours observing of a source at -45 deg declination, with a resolution of 30 arcsec. The constraints have had no effect on the layout and so this can be moved as is to another site. I show it in two locations – Red and Green. The minimum and maximum baselines are 29m and 1904m respectively.

The elements are numbered as follows – the first six elements are labeled in recommended order of deployment as XNTD6, and the next twentyfour are labeled in azimuth, starting from the north and going clockwise. The elements in XNTD6 have been chosen to give predominantly short spacings and a reasonable synthesized beam for a long integration, but another subset could be substituted.

Figure 7 XNTD30 RED and GREEN - 30 12m diameter antennas giving 30 arcsecond resolution for a 300MHz band with upper frequency 1.4GHz

The configuration XNTD30 can be grown to double resolution and collecting area (XNTD60) by adding 30 more antennas while keeping an acceptable Gaussian beam. Going to higher resolutions, such as 10 arcsecond or beyond, produces a non-Gaussian beam, as the core of short spacings comes to dominate the sensitivity function, producing a plateau in the naturally weighted beam. The coverage is still excellent, though and so little deconvolution would be required, though some loss in sensitivity would be incurred.

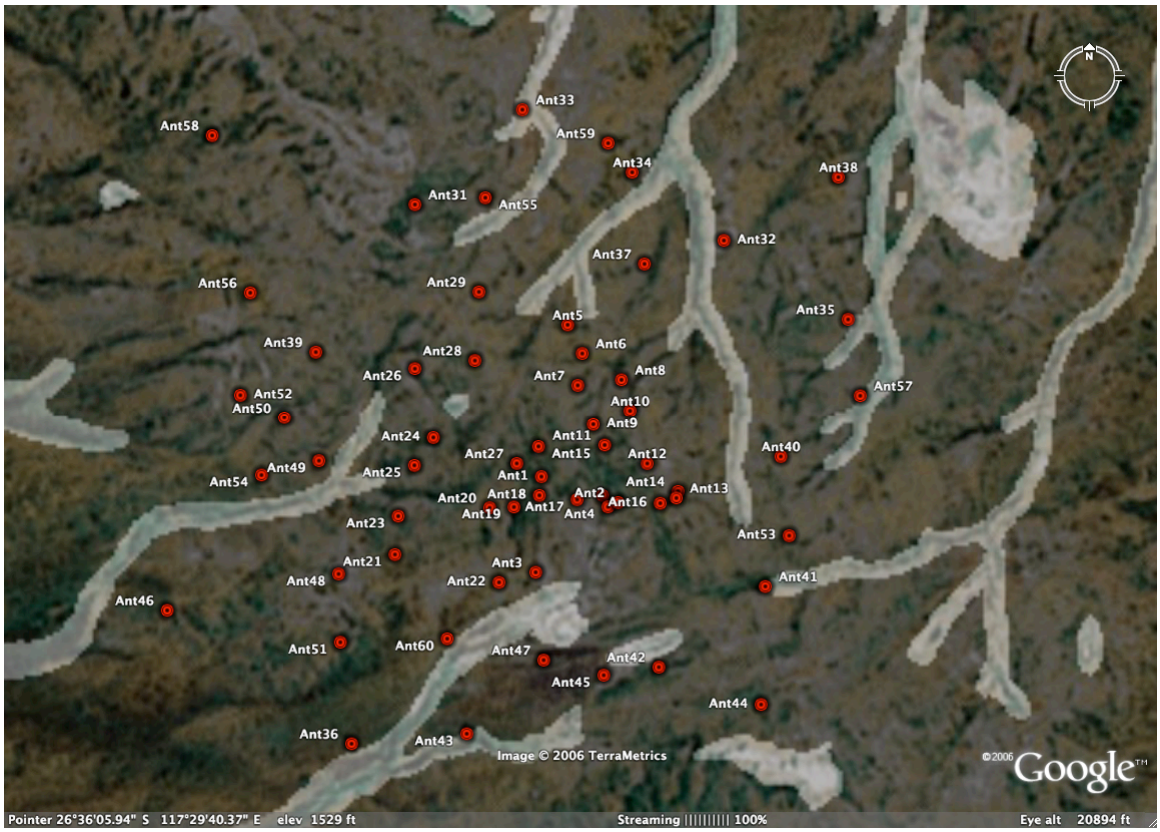

Figure 8 XNTD60/RED - 30 antennas added to XNTD30/RED giving 15 arcsecond resolution. The maximum baseline is about 5km.

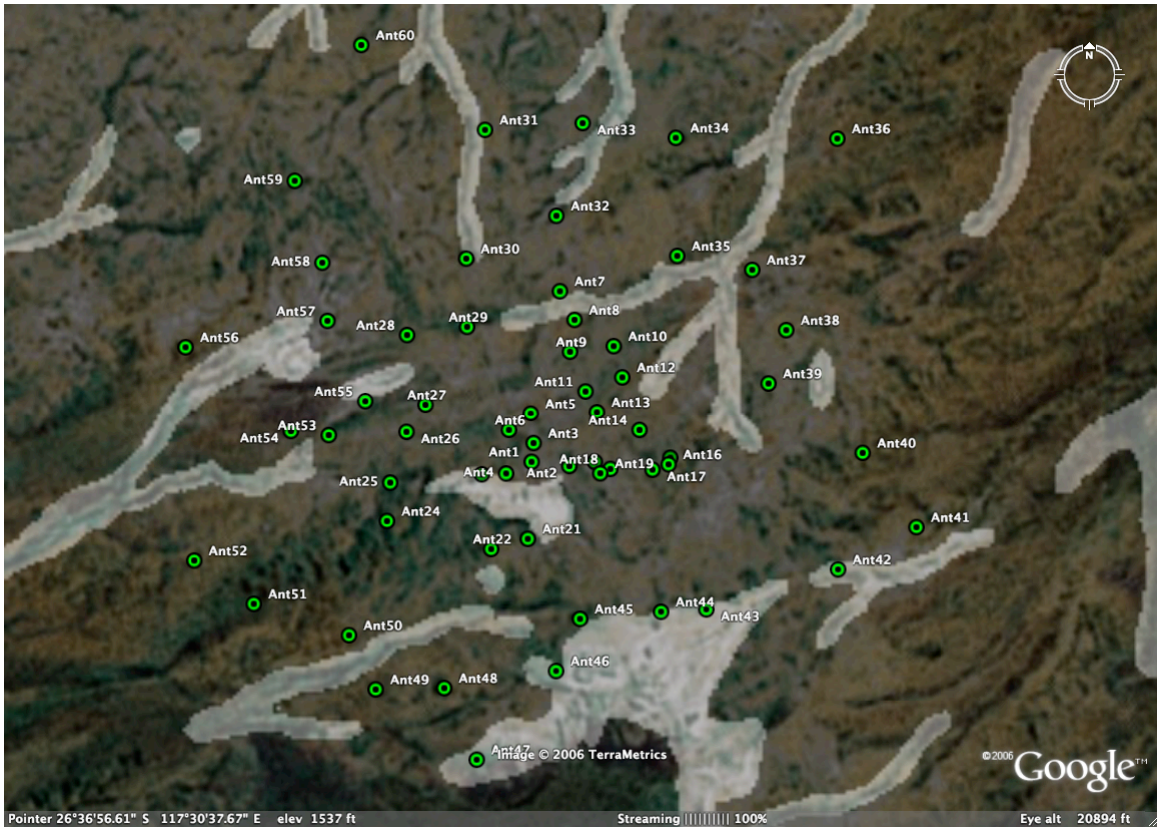

Figure 9 XNTD60 on GREEN. There are a few remaining problem areas to be resolved such as Ant 43-46

Overall, the GREEN location is superior to the RED location because of two factors:

1. RED is located along the ridge line whereas GREEN is about 20 – 25m lower. As a result, GREEN has slightly more terrain protection from RFI originating on the road (Ron Beresford, private communication).
2. RED has more weathered and exposed rock, probably leading to more trenching constraints. GREEN also has exposed rock in some areas but there are fewer limitations arising.

A spiral configuration is also presented. The PSF for this has very noticeable wings, and as a consequence deconvolution of the continuum takes more major cycles, and deconvolution of the spectral line may be necessary.

Figure 10 XNTD30SPIRAL/RED - Spiral armed array with 30 arcsecond resolution

The difference in imaging performance between the optimized and the spiral configurations can be illustrated by a simulation. I have simulated an 8 hour observation of a single field with both XNTD30 and XNTD30SPIRAL. The field was cleaned to a level of 50uJy/beam.

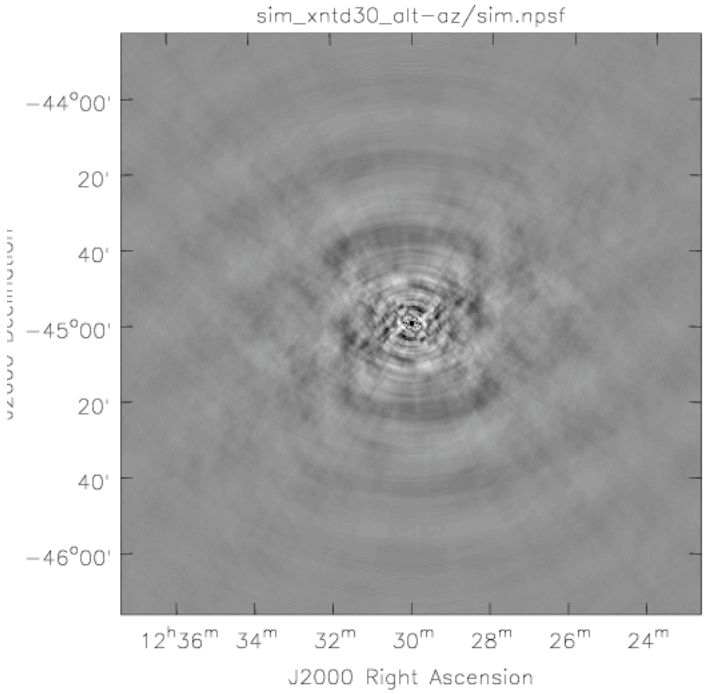

Figure 11 XNTD30 8 hour integration naturally weighted PSF. Display range -1% to +1%.

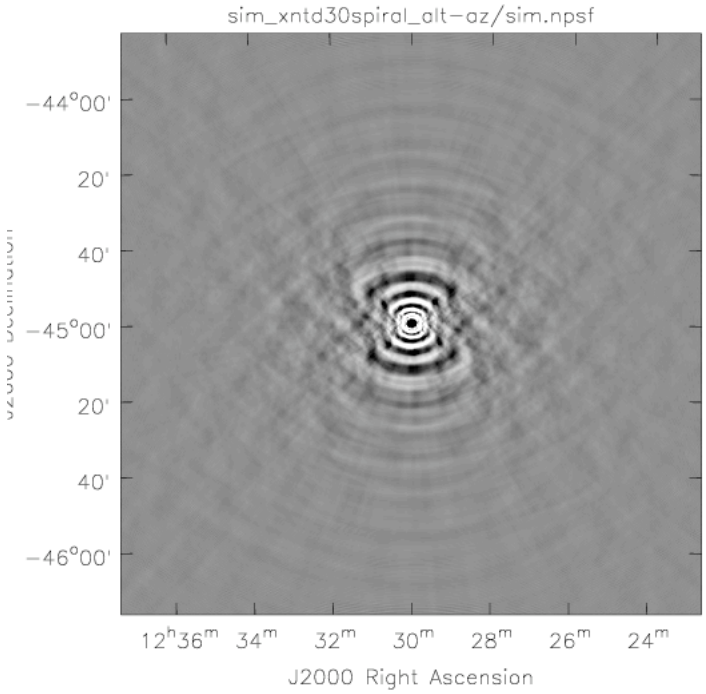

Figure 12 XNTD30SPIRAL 8 hour integration naturally weighted PSF. Display range -1% to +1%.

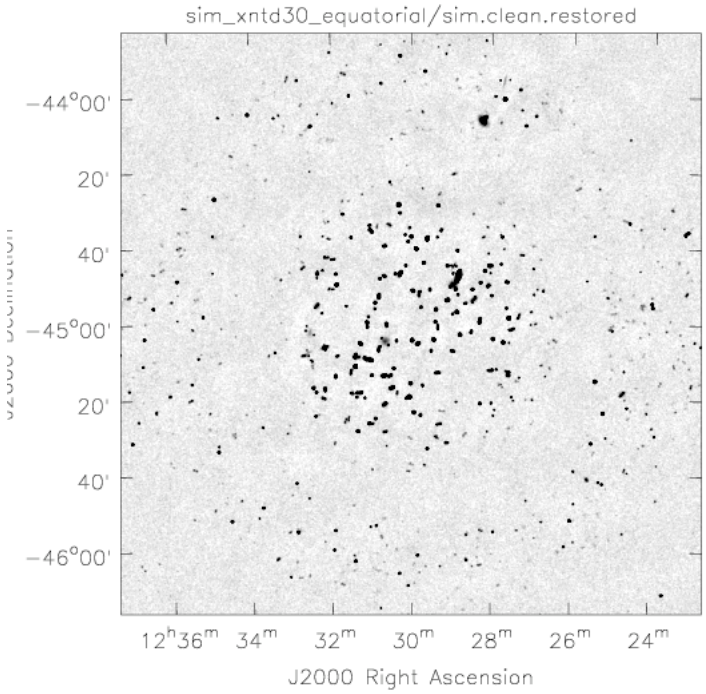

Figure 13 XNTD30 8h integration on simulated single field. Display range -10 to +100 uJy/beam

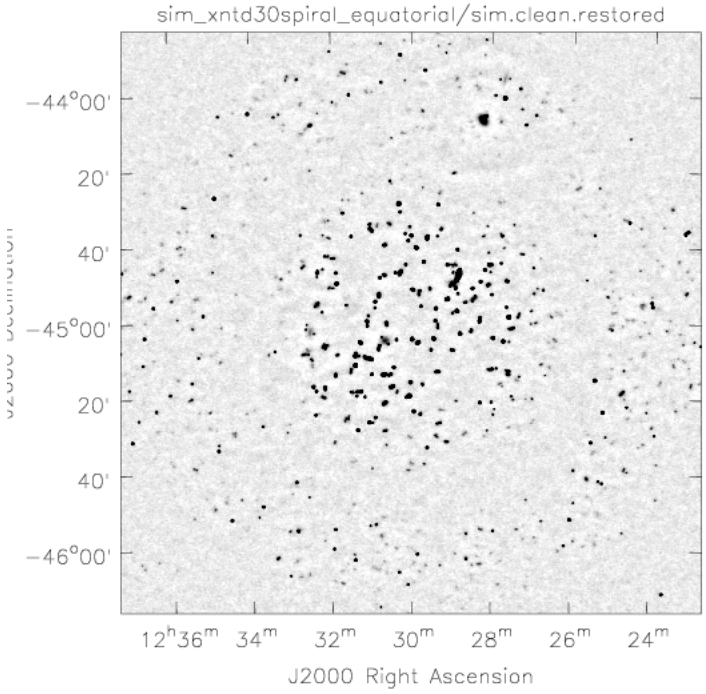

Figure 14 XNTD30SPIRAL 8h integration on simulated single field. Display range -10 to +100 uJy/beam

6. Contingencies

In this document, I have made assumptions about requirements that are still yet to be agreed by the science community. We can expect these questions to be resolved at the upcoming xNTD science meeting. Given that, the configurations presented in current document, XNTD60 GREEN, should be taken as just a strawman that may be changed on further review.

The following changes may be desired:

- Different sequencing of antenna construction in XNTD6.
- Moderate expansion up to 20 or 10 arcsecond resolution. The current site can accommodate such changes but the computing scales as the square (or worse) of the baseline length.
- On a longer term, expansion to baselines up to 10km or possibly more, yielding a maximum resolution of about 5 arcsecond on the current site.
- Use of a scale free configuration such as the log-spiral if more than one resolution is required.
- Modification of any antenna location by up to a few dish diameters. The exceptions to this are those antennas producing the shortest spacings – antennas 15-20.
- Down scoping to fewer antennas would require a re-evaluation of the resolution goal. For example, 20 antennas would probably require a fall back to 45 arcsec resolution.

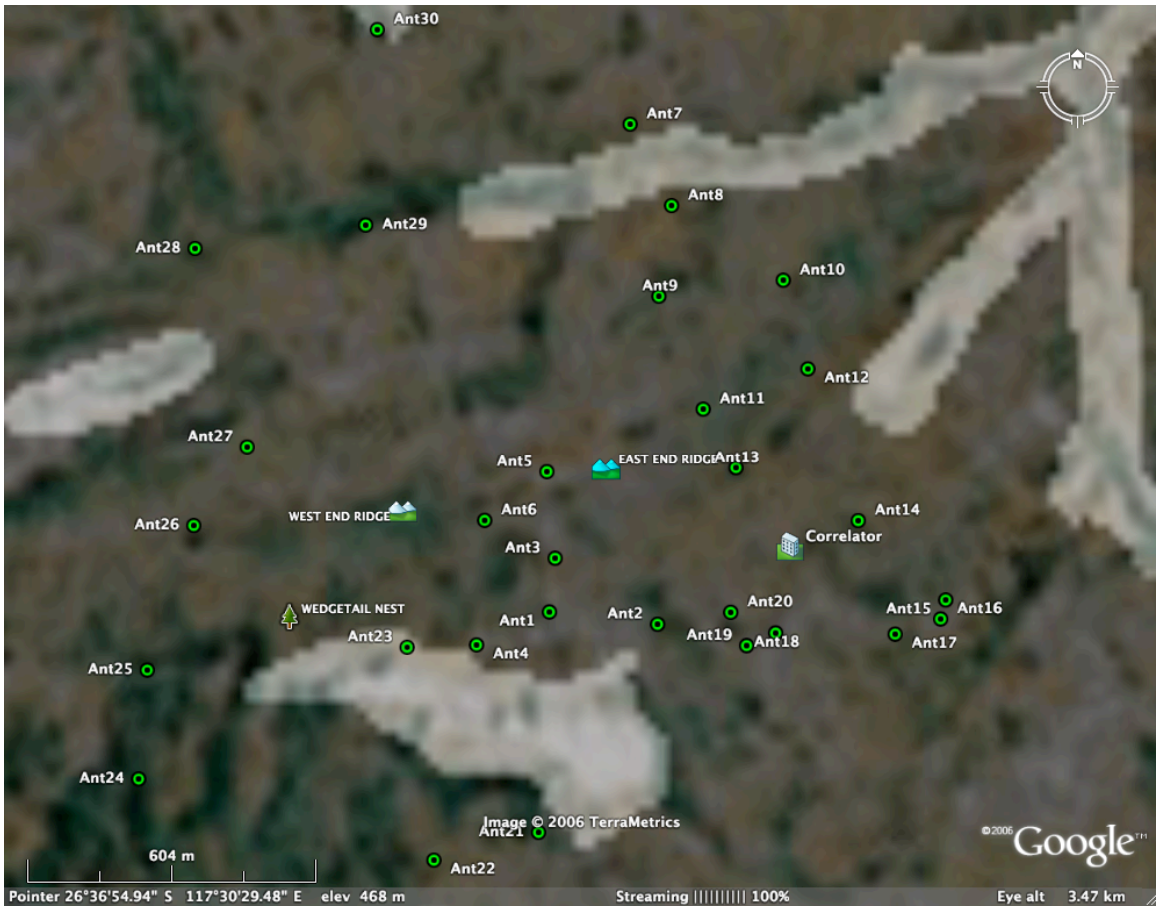

Figure 15 XNTD30/GREEN layout, showing rocky ridge, Wedgetail nest, and possible correlator building location.

Figure 16 Looking north from Ant3 at GREEN. Ant 5 is located just the other side of the rocky ridge seen on the horizon.

Acknowledgements

I thank Mattieu de Villiers for making AntConfig available and for adding features as requested. This work could not have proceeded as quickly without this resource.

References

Boone, P, 2001, Astron. Astrophys., 377, 368-376.

Cornwell, T.J., 1988, Astron. Astrophys., 202, 316

Cornwell, T.J., Holdaway, M.H., Uson, J.M., 1993, Astron. Astrophys., 271, 697-713

Cornwell, T.J., 2005, ATNF SKA memo series 1,
http://www.atnf.csiro.au/projects/ska/Memoseries.html

Johnston, S., 2005, ATNF SKA memo series 3,
http://www.atnf.csiro.au/projects/ska/Memoseries.html

Johnston, S., 2006, ATNF SKA memo series 7,
http://www.atnf.csiro.au/projects/ska/Memoseries.html

Keto, E. 1997, ApJ, 475, 843-852, 1997

Oberoi, D., 2006, "Proposed sites for LFD and xNTD", LFD memo, 30 June 2006.

Staveley-Smith, L., 2006, ATNF SKA memo series 6,
http://www.atnf.csiro.au/projects/ska/Memoseries.html

Appendix A: XNTD coordinates

The recommended antenna locations are stored in:

http://sourcecode.atnf.csiro.au/repos/NTD/configurations/configs/xNTD/xntd60.green.txt

The following table gives the antenna coordinates. The X,Y positions are those for the GREEN location.

NAME	LONGITUDE	LATITUDE	X	Y	ARRAY
Ant1	117.507540	-26.618147	1652.9	1940.8	XNTD6
Ant2	117.509776	-26.618368	1876.5	1965.4	XNTD6
Ant3	117.507658	-26.617154	1664.7	1829.6	XNTD6
Ant4	117.506028	-26.618763	1501.7	2009.6	XNTD6
Ant5	117.507488	-26.615554	1647.7	1650.7	XNTD6
Ant6	117.506198	-26.616456	1518.7	1751.6	XNTD6
Ant7	117.509218	-26.609065	1820.7	925.0	XNTD30
Ant8	117.510082	-26.610581	1907.1	1094.6	XNTD30
Ant9	117.509815	-26.612269	1880.4	1283.3	XNTD30
Ant10	117.512406	-26.611975	2139.5	1250.5	XNTD30
Ant11	117.510735	-26.614375	1972.4	1518.8	XNTD30
Ant12	117.512913	-26.613625	2190.2	1435.0	XNTD30
Ant13	117.511411	-26.615478	2040.0	1642.2	XNTD30
Ant14	117.513933	-26.616458	2292.2	1751.8	XNTD30
Ant15	117.515760	-26.617931	2474.9	1916.6	XNTD30
Ant16	117.515656	-26.618282	2464.5	1955.8	XNTD30
Ant17	117.514702	-26.618560	2369.1	1986.9	XNTD30
Ant18	117.512204	-26.618521	2119.3	1982.6	XNTD30
Ant19	117.511606	-26.618752	2059.5	2008.4	XNTD30
Ant20	117.511286	-26.618147	2027.5	1940.7	XNTD30
Ant21	117.507317	-26.622222	1630.6	2396.5	XNTD30
Ant22	117.505140	-26.622760	1412.9	2456.6	XNTD30
Ant23	117.504586	-26.618807	1357.5	2014.6	XNTD30
Ant24	117.498960	-26.621284	794.9	2291.6	XNTD30
Ant25	117.499153	-26.619249	814.2	2064.0	XNTD30
Ant26	117.500119	-26.616558	910.8	1763.0	XNTD30
Ant27	117.501248	-26.615078	1023.7	1597.6	XNTD30
Ant28	117.500153	-26.611384	914.2	1184.4	XNTD30
Ant29	117.503714	-26.610954	1270.3	1136.3	XNTD30
Ant30	117.503665	-26.607345	1265.4	732.6	XNTD30
Ant31	117.504774	-26.600521	1376.3	-30.5	XNTD60
Ant32	117.509007	-26.605071	1799.6	478.4	XNTD60
Ant33	117.510567	-26.600154	1955.6	-71.6	XNTD60
Ant34	117.516090	-26.600936	2507.9	15.9	XNTD60
Ant35	117.516175	-26.607192	2516.4	715.6	XNTD60
Ant36	117.525684	-26.600966	3467.3	19.3	XNTD60
Ant37	117.520625	-26.607930	2961.4	798.0	XNTD60
Ant38	117.522636	-26.611125	3162.5	1155.5	XNTD60
Ant39	117.521583	-26.613949	3057.2	1471.3	XNTD60

Ant40	117.527175	-26.617675	3616.4	1887.9	XNTD60
Ant41	117.530360	-26.621607	3934.9	2327.7	XNTD60
Ant42	117.525707	-26.623842	3469.6	2577.7	XNTD60
Ant43	117.517892	-26.625953	2688.1	2813.8	XNTD60
Ant44	117.515208	-26.626076	2419.7	2827.4	XNTD60
Ant45	117.510409	-26.626456	1939.8	2870.0	XNTD60
Ant46	117.508989	-26.629206	1797.8	3177.6	XNTD60
Ant47	117.504286	-26.633906	1327.5	3703.2	XNTD60
Ant48	117.502358	-26.630123	1134.7	3280.2	XNTD60
Ant49	117.498288	-26.630200	727.7	3288.7	XNTD60
Ant50	117.496703	-26.627334	569.2	2968.2	XNTD60
Ant51	117.491040	-26.625676	2.9	2782.8	XNTD60
Ant52	117.487505	-26.623381	-350.6	2526.0	XNTD60
Ant53	117.495500	-26.616733	448.9	1782.5	XNTD60
Ant54	117.493256	-26.616517	224.5	1758.4	XNTD60
Ant55	117.497671	-26.614888	666.0	1576.2	XNTD60
Ant56	117.486997	-26.612026	-401.4	1256.2	XNTD60
Ant57	117.495428	-26.610634	441.7	1100.5	XNTD60
Ant58	117.495125	-26.607555	411.4	756.1	XNTD60
Ant59	117.493496	-26.603222	248.5	271.5	XNTD60
Ant60	117.497432	-26.596020	642.1	-533.9	XNTD60

Appendix B: Details of *harry*

The array optimization program, *harry*, finds antenna locations on a plane that match the naturally weighted PSF to a Gaussian, as described in the main text. It is implemented in python, using Scipy libraries for FFTs. The derivative of the objective function with respect to the unknown antenna locations is calculated straightforwardly. It is necessary to use FFTs to perform the transforms to and from image space since a direct summation is too slow for the typical image size and number of samples. The gradient is calculated using the derivative theorem. The gradient is then used as to update the antenna locations, with the exact scaling being determined by a line search in the direction of the update. Since the objective function is non-quadratic in the antenna locations, the convergence of this cavalier type of approach is not at all certain. Nevertheless, it does give good results most of the time as evidenced by a more or less monotonic decrease in the value of the objective function.

The bulk of the computation load is incurred in moving the visibility data to and from the regular grid used for the FFT. Although we use a simple nearest neighbor gridding, even this contains multiple additions to the same memory location and cannot be done in an efficient way, especially in python.

```
def griduv(self, b, coords, gridsize=100):
        grid=ndarray(shape=[gridsize,gridsize], dtype=float)*0.0
```

```
        nsamples=b.shape[1]
        for i in range(nsamples):
                grid[coords[0,i],coords[1,i]]=grid[coords[0,i],coords[1,i]]+1.0
        return grid

def degriduv(self, b, coords, (gridx, gridy)):
        nsamples=b.shape[1]
        values=ndarray(shape=[2, nsamples], dtype=float)*0.0
        values[0,...]=gridx[coords[0,...],coords[1,...]]
        values[1,...]=gridy[coords[0,...],coords[1,...]]
        return values
```

Below I show an example of optimizing 20 antennas for maximum baselines of about 200m. The array is located at latitude -26 (Mileura), and is observing a source at declination -45 for twelve hours. The fractional bandwidth is 20%. The penultimate image on each figure is the quadrature of the gradients with respect to *x* and *y*. The last image is the residual PSF centered at the corners. In this example, *harry* essentially converges in about 30 iterations.

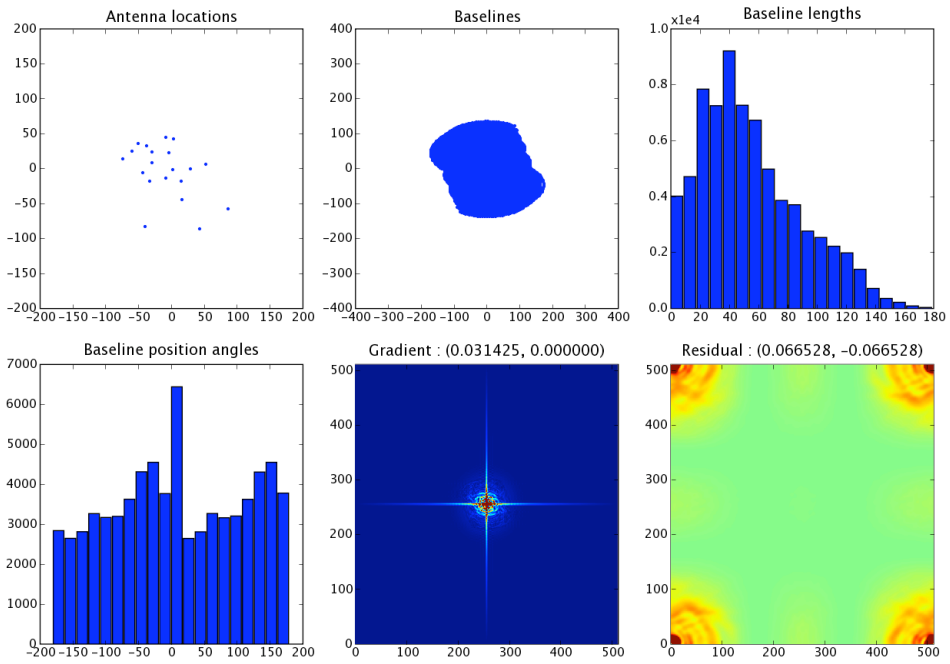

Figure 17 Initial state of optimization - antenna locations have been chosen at random

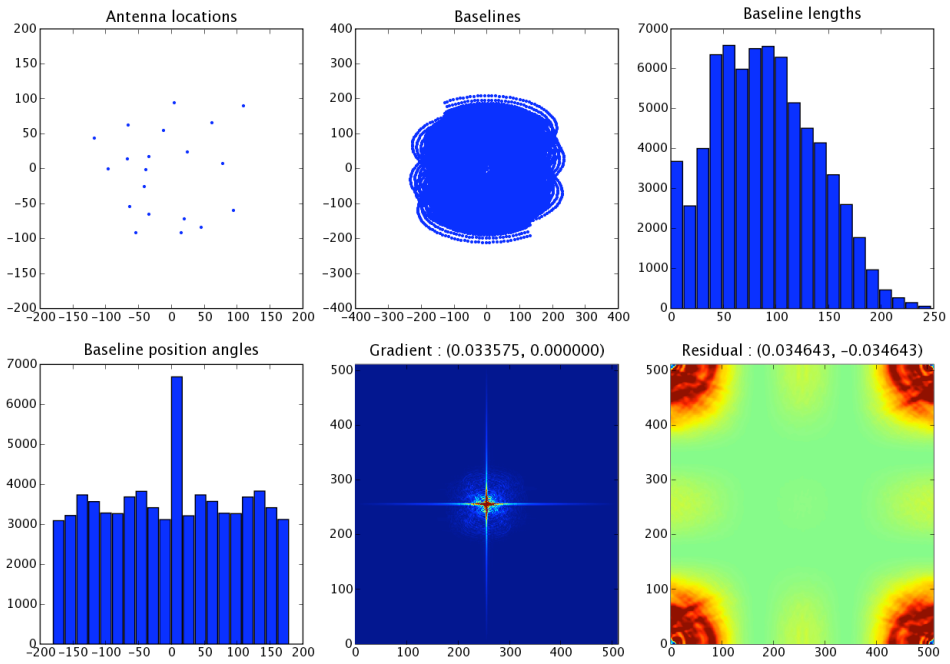

Figure 4 State after 50 iterations - the array has spread out as desired and the baselines are uniform in position angle. The typical sidelobe level has decreased by a factor of two.